

See discussions, stats, and author profiles for this publication at: <https://www.researchgate.net/publication/281589533>

Size-Dependent Appearance of Intrinsic Oxq “Activated Oxygen” Molecules on Ceria Nanoparticles

ARTICLE *in* CHEMISTRY OF MATERIALS · AUGUST 2015

Impact Factor: 8.35 · DOI: 10.1021/acs.chemmater.5b02426

CITATION

1

READS

13

2 AUTHORS, INCLUDING:



Xing Huang

University of Kentucky

8 PUBLICATIONS 82 CITATIONS

[SEE PROFILE](#)

Size-Dependent Appearance of Intrinsic O_x^q "Activated Oxygen" Molecules on Ceria Nanoparticles

Xing Huang^{*,†} and Matthew J. Beck^{*,†,‡}

[†]Department of Chemical & Materials Engineering and [‡]Center for Computational Sciences, University of Kentucky, Lexington, Kentucky 40506, United States

S Supporting Information

For the past 40 years, efforts to promote the catalytic activity of ceria (CeO_2) have focused on increasing the number of O-vacancy-related, catalytically active surface sites by designing or discovering reduced CeO_2 materials with increased concentrations of O vacancies. This approach is fundamentally limited in terms of the absolute density of active sites that can be realized. From a stoichiometric perspective, no more than 25% of all O lattice sites can be vacant before CeO_2 transforms to catalytically inert Ce_2O_3 , and from a kinetic perspective, as O vacancies have a positive formation enthalpy of ~ 4.7 eV,¹ even at elevated temperatures the number of O vacancies is limited. Here we report results showing that, below a critical size, the surfaces of oxidized ceria nanoparticles (CNPs) are intrinsically inundated with molecular oxygen species analogous to previously described "activated oxygen" molecules. This suggests that sufficiently small "super-oxidized" CNPs can be fabricated with densities of surface active sites of up to 1 per surface O lattice site (~ 12 sites per nm^2).

CeO_2 is widely applied as a key component in three-way catalysts for the treatment of automotive exhaust and as an industrially important redox catalyst and/or catalyst support for CO oxidation,² the water–gas shift reaction,³ photocatalytic water splitting,⁴ and in solid oxide fuel cells.⁵ Since the 1970s, extensive efforts have been undertaken to understand the mechanism of ceria's redox activity and to increase the activity, selectivity, and oxygen storage capacity (OSC) of ceria materials. While the precise mechanism of ceria's catalytic activity remains under debate, it is widely accepted that bulk and surface O vacancies (and associated Ce^{3+} cations) are key chemical and structural features dictating ceria's catalytic activity. Beyond this, some researchers argue that it is, in fact, "activated oxygen"—negatively charged molecular oxygen species formed by adsorbing ambient oxygen at surface O-vacancy sites—that are the catalytically active structures on ceria surfaces.^{6–8} Driven by studies showing that the O-vacancy formation energy decreases with decreasing particle size,⁹ significant effort has focused on ceria nanostructures, aiming to achieve enhanced activity by minimizing O-vacancy formation energies, and therefore maximizing the number of O-vacancy-related active sites. Critically, many of these efforts, constrained by the assumption of O-vacancy-controlled catalytic mechanisms, have been limited to reduced or partially reduced ceria materials.

In contrast, over the past five years, experimental and computational results have shown that ceria nanoparticles with diameters less than ~ 10 nm can achieve dramatically higher OSC than bulk ceria materials without requiring the

prerequisite formation of explicit oxygen vacancies. In 2010, Xu et al.¹⁰ reported enhanced low-temperature OSC for ultrasmall CNPs (diameters < 10 nm) and used electron paramagnetic resonance spectroscopy (EPR) to tie this enhanced OSC to surface adsorbed superoxo (O_2^-) species. A subsequent computational study based on density functional theory (DFT) by Kullgren et al.¹¹ explicitly investigated the stability of "understoichiometric" CNPs—CNPs with intrinsic Ce^{3+} ions due to nonstoichiometric corners and edges but free of explicit oxygen vacancies—exposed to O_2 molecules. This study showed that understoichiometric CNPs are stabilized by the adsorption of O_2^- species at intrinsic Ce^{3+} ion sites, and that these superoxo species could explain experimental observations of enhanced OSC for small CNPs at low temperatures. In addition, a separate computational work¹² broadly exploring variously shaped ultrasmall CNPs as a function of surface oxygen concentration showed that "activated oxygen"—negatively charged molecular oxygen species (O_x^q molecules, $x = 2, 3, -2 \leq q \leq 0$)—are an intrinsic feature of thermodynamically stable CNP surface structures for CNPs below a critical size.

In this communication we report results of IR absorption spectroscopy experiments directly probing for the presence of surface O_x^q molecules on CNPs. We report the particle size-dependent appearance of stable, surface-adsorbed O_x^q molecules analogous to previously reported "activated oxygen" molecules. CNP cubes and polyhedrons in two different size regimes ("ultrasmall", ~ 5 nm in diameter, and "small", ~ 15 –30 nm in diameter) were synthesized and imaged with transmission electron microscopy (TEM). After identical annealing treatments in a controlled O_2 -containing environment, IR absorption spectroscopy reveals the presence of surface O_x^q molecules on "ultrasmall" samples but not on "small" samples. These results demonstrate the existence of a transition in the nature of similarly shaped CNPs as a function of nanoparticle size and show that stable "ultrasmall" CNPs can be directly fabricated with a high surface density of intrinsically present surface O_x^q molecules.

Figure 1 shows representative postsynthesis TEM images of the four different CNPs considered here. Both "ultrasmall" and "small" cubic CNPs (Figure 1a,c) exhibit a clear predominance of {200} exposed facets featuring lattice spacing of 0.27 nm, along with occasional {220} facets featuring lattice spacing of

Received: June 20, 2015

Revised: August 24, 2015

Published: August 24, 2015

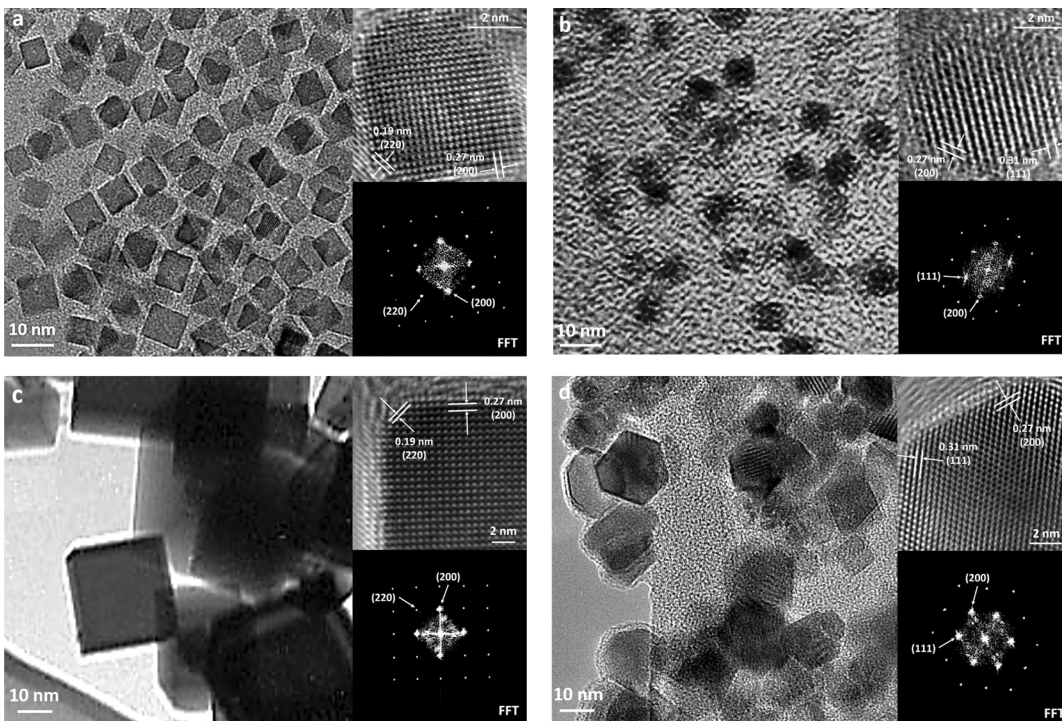


Figure 1. (a) TEM image of 5 nm cubic CNPs (upper inset, high resolution image of a single particle, and lower inset, FFT analysis of this particle showing that it is oriented along the [100] zone axis); (b) TEM image of 5 nm polyhedral CNPs (upper inset, high resolution image of a single particle, and lower inset, FFT analysis of this particle showing that it is oriented along the [110] zone axis); (c) TEM image of 30 nm cubic CNPs (upper inset, high resolution image of a partial single particle, and lower inset, FFT analysis of this particle showing that it is oriented along the ([100] zone axis); and (d) TEM image of 15 nm polyhedral CNPs (upper inset, high resolution image of a partial single particle, and lower inset, FFT analysis of this particle showing that it is oriented along the [110] zone axis).

0.19 nm. “Ultrasmall” cubic CNPs (Figure 1a) exhibit side lengths of ~5 nm, while “small” cubic CNPs exhibit side lengths of ~20–30 nm. Fast Fourier transform (FFT) analysis of both “ultrasmall” and “small” cubic CNPs shows a typical single crystal domain pattern of CeO_2 , confirming the formation of well-crystallized cubes oriented along the [110] zone axis (see lower insets in Figure 1a,c). Polyhedral CNPs (Figure 1b,d) exhibit combinations of {200} exposed facets featuring lattice spacing of 0.27 nm and {111} exposed facets featuring lattice spacing of 0.31 nm, with “ultrasmall” polyhedral CNPs having diameters of ~5 nm versus ~15 nm for “small” polyhedral CNPs. FFT analysis of both “ultrasmall” and “small” polyhedral CNPs shows the typical single crystal reflections expected of a CeO_2 crystal oriented along the [100] zone axis (see lower insets in Figure 1b,d).

Note that TEM images clearly indicate the presence of residual organic materials on all postsynthesis CNP samples excluding 30 nm cubic CNPs. To remove any adsorbed surface species and achieve a common “clean” initial state, all CNPs were annealed at 900 °C in pure Ar gas. All CNPs were then held at 650 °C in an oxidizing atmosphere of mixed O₂ and Ar gas to obtain fully oxidized CNPs (see Supporting Information for details).

Figure 2 shows the collected IR absorption spectra from all four CNP samples after the two-stage reduction in Ar and then oxidation in mixed Ar and O₂ annealing (see Supporting Information for details). None of the IR spectra reveal absorption peaks at high wavenumbers (above 2800 cm⁻¹), and all samples exhibit strong IR absorption at and below 600 cm⁻¹ that is associated with bulk Ce–O bonds. In contrast to these regions of similar absorption, there is a marked difference

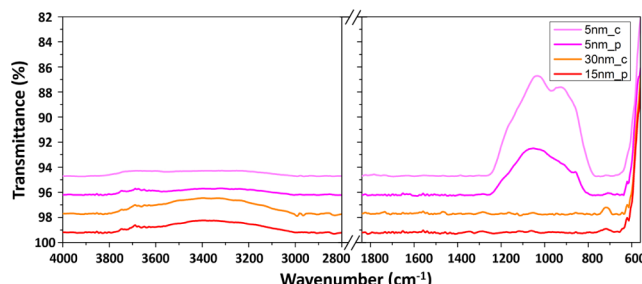


Figure 2. IR absorption spectra of 5 and 30 nm cubic CNPs (5nm_c and 30nm_c in the figure) as well as 5 and 15 nm polyhedral CNPs (5nm_p and 30nm_p) after first being reduced at 900 °C and then oxidized at 650 °C.

in absorption behavior between “ultrasmall” and “small” CNPs of both shapes between 1200 and 800 cm⁻¹.

IR absorption is sensitive to the vibrational states of chemical bonds in a system and, therefore, is sensitive to both chemical and configurational information. As TEM images show that all CNPs are crystalline cubic fluorite and postsynthesis high-temperature annealing is expected to remove any surface adsorbates present prior to annealing in the mixed Ar and O₂ gas atmosphere, differences in postannealing IR absorption must be attributed to differences in CNP behavior during annealing in Ar + O₂ or during postannealing exposure to room air. It is widely accepted that environmental species, particularly small molecules, will adsorb on CNPs. While oxygen can be expected to adsorb both during Ar + O₂ annealing and when exposed to room air, additional airborne species—including CO, CO₂, and H₂O-related species—are also known to adsorb

on CNPs. Of these species, all except various O_x^q molecules are known to exhibit IR absorption outside of the 1200 to 800 cm^{-1} range (not observed for any CNP samples), and only O_x^q molecules are known to exhibit IR absorption within that range (as observed here for “ultrasmall” CNPs).

Close examination of the 1200 to 800 cm^{-1} region indicates that the observed peaks are compound peaks (see Figure 3).

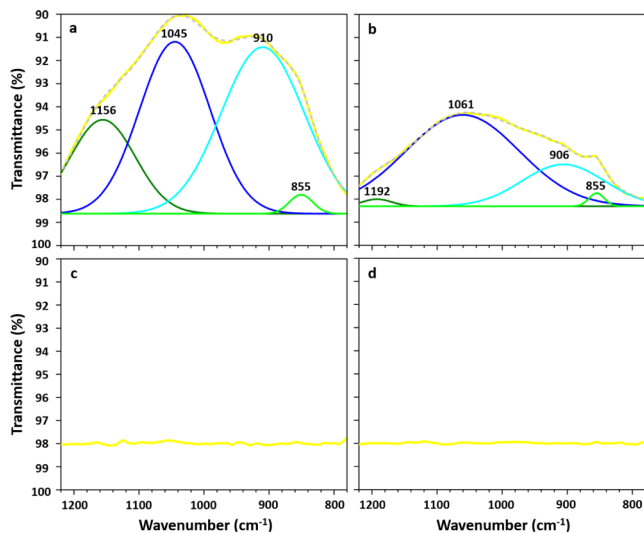


Figure 3. Zoom-in region of IR absorption spectra of all postannealing CNPs between 1200 and 800 cm^{-1} : (a) 5 nm cubic CNPs; (b) 5 nm polyhedral CNPs; (c) 30 nm cubic CNPs; and (d) 15 nm polyhedral CNPs.

Gaussian fitting yields a best fit with four contributing peaks: ~ 1175 , ~ 1050 , ~ 910 , and $\sim 855 \text{ cm}^{-1}$. By comparison to previously reported IR absorption and Raman spectroscopy studies of oxygen molecules adsorbed on bulk ceria surfaces (see summary in Table 1), we can identify these component

Table 1. Experimental IR/Raman Vibrational Frequencies for Adsorbed Molecular Oxygen Species on Bulk CeO_2

measured frequency [cm^{-1}]	assignment	ref
1128, 1126	O_2^-	13–18
1139–1127 (Raman)		19, 20
883	O_2^{2-}	13, 15, 18
890–831 (Raman)		19, 20
1126, 1104, 1096	O_3 sym. stret.	21, 22
1035, 1018–1015, 1012–1008, 1004	O_3 anti. stret.	21, 22
792	O_3^- sym. stret.	22
772	O_3^- anti. stret.	22

peaks as arising from superoxo (O_2^-), ozone (O_3), and peroxy (O_2^{2-}) species, respectively. Peaks at ~ 910 and $\sim 855 \text{ cm}^{-1}$ are attributed to two different adsorption geometries of peroxy species. As can be seen, there is excellent agreement between the present results and previous identifications of peaks for molecular oxygen species adsorbed on ceria. A small systematic blue-shift of absorption peaks is present and likely indicates slightly tighter binding of O_x^q molecules on CNP surfaces compared to bulk surfaces.

On the basis of these findings we conclude that molecular oxygen species (O_x^q molecules) are present on “ultrasmall” nanoparticles, both cubic and polyhedral, after exposure to appropriate environments. Further, we note that these surface

groups are stable when exposed to air and are not displaced by carbon or hydrogen containing species at room temperature. In contrast, O_x^q molecules are not present on larger (~ 15 –30 nm) cubic or polyhedral nanoparticles after either annealing in an oxidizing environment or exposure to room air.

In other words, both cubic and polyhedral CNPs have undergone a size-induced transition with regards to the presence of surface O_x^q molecules. What is the origin of this effect? Conventional theories hold that O_x^q molecules²³ appear on CNPs after being adsorbed at previously formed surface O vacancies. Previous calculations have shown that the O-vacancy formation energy is smaller on CNPs than bulk ceria and, in fact, may decrease with decreasing CNP size.⁹ As these calculations estimate formation energies of surface O vacancies as low as $\sim 0.5 \text{ eV}$ for “ultrasmall” CNPs and $\sim 1.9 \text{ eV}$ for “small” CNPs,²⁴ annealing at 900 °C in pure Ar gas should be sufficient to generate surface O-vacancies on both “small” and “ultrasmall” CNPs. If this were the case, then both “small” and “ultrasmall” CNPs should exhibit nonzero adsorption of O_x^q molecules once exposed to an oxidizing atmosphere of mixed Ar gas and O_2 gas. In fact, given the uniform 900 °C annealing in pure Ar gas and the binary finding of no (as opposed to lower concentrations of) O_x^q molecules on “small” CNPs versus the clear presence of O_x^q molecules on “ultrasmall” CNPs, it is difficult to explain the present results on the basis of the nature of surface O vacancies—which should be present on both “small” and “ultrasmall” CNPs—at all.

Kullgren et al.¹¹ have put forward an explanation for previous experimental observations of adsorbed surface oxygen species based on their results showing that O_2^- species stabilize understoichiometric CNPs by adsorbing at surface Ce^{3+} ions. They conclude that the number of adsorbed O_2^- species should be expected to equal to the number of Ce^{3+} ions present in undecorated CNPs, leading to “super-oxidized” CNPs. Kullgren et al.¹¹ then show that undecorated CNPs are understoichiometric at any size, with the number of Ce^{3+} ions proportional to the side length of the nanoparticle. Therefore, though the relative degree of understoichiometry decreases with nanoparticle size, CNPs of all sizes will exhibit O_2^- adsorption, with larger CNPs adsorbing larger absolute numbers of O_2^- species. While the magnitude of superoxidation due to this effect in terms of measured OSC (that is, the relative increase in O content due to the presence of surface adsorbed O_2^- species) will decrease with increasing particle size¹¹, this should not be the case for IR absorption by such surface groups. That is, as IR spectroscopy is sensitive to the absolute number of surface oxygen species, not their number relative to the number of O atoms within the CNP itself, the Kullgren findings imply that O_2^- species should be observed by IR on both “small” and “ultrasmall” CNPs, in contrast to the present findings.

A later computational study¹² similarly finds that anionic surface oxygen species stabilize small CNPs. This study, though, finds that O_x^q surface groups are only necessary to stabilize nonstoichiometric CNP surfaces, edges, and corners below a critical nanoparticle size. This critical size is reached when the surface-to-volume ratio for a given CNP becomes high enough that terminating nonstoichiometric CNP surfaces [e.g., $\text{Ce}(001)$], edges, and corners with atomic oxygen in the 2– charge state would require some number of Ce atoms to be oxidized beyond Ce^{4+} . Larger CNPs can sustain atomic oxygen (O^{2-}) terminated surfaces without requiring the presence of Ce atoms oxidized beyond Ce^{4+} because, as widely reported,²⁵ bulk ceria exhibits a finite concentration of (bulk) O vacancies at

finite temperature. Therefore, in this picture, CNPs are thermodynamically stable with O_x^q -terminated surfaces only when smaller than a critical size.

On the basis of these prior calculations,¹² both the “ultrasmall” cubic and polyhedral CNPs in the present study should be below the critical size while both the “small” cubic and polyhedral CNPs should be above the critical size. Hence, previous calculations¹² directly predict that—Independent of the thermodynamics and kinetics of surface O vacancies—clean “ultrasmall” CNPs exposed to O_2 will be thermodynamically stable when densely covered with O_x^q molecules and that clean “small” CNPs similarly exposed will be thermodynamically stable with only atomic oxygen (and no O_x^q molecules) at CNP surfaces. The experimental findings reported here represent a direct test of this prediction, and experimental results agree completely with computational predictions.

It should be noted that the present results cannot be used to directly determine the relative surface concentrations of different O_x^q molecules. This is because the relative area enclosed by absorption peaks is a convolution of the number of absorbing species and the absorption strength of each species. The absorption strength is related to the magnitude of the charge dipole present in specific adsorbed species, a value that will certainly vary among different O_x^q molecules. CNPs with mixed O_x^q -group terminations were considered in previous calculations,¹² and different relative concentrations and distributions of O_x^q molecules were found to be stable, depending on the size and shape of the CNP. The dependence of O_x^q molecule distributions on CNP shape is consistent with the present finding of different relative O_x^q absorption intensities for cubic and polyhedral CNPs.

The present findings contribute to a growing body of literature suggesting a new route to improving the activity of ceria-based catalysts. That is, instead of seeking to increase the density of catalytically active surface sites by maximizing the formation of surface O vacancies—necessarily an uphill thermodynamic process requiring reducing environments and elevated temperatures—active site densities can be dramatically increased for sufficiently small CNPs treated in oxidizing environments. Such nanoparticles take advantage of the size-dependent emergence of surfaces intrinsically covered with O_x^q molecules. In fact, because O_x^q -covered surfaces are stable structures,^{11,12} these superoxidized, “activated-oxygen”-covered CNPs will exhibit maximum density of active sites at low temperatures and in oxidizing environments.

As a final note, the size-dependent transformation in nanoparticles surface configuration that underlies the results of this study are likely not limited to cerium dioxide nanoparticles. In general, any metal oxide material should exhibit a critical size below which O_x^q -terminated surfaces are preferred over surface terminated with doubly negative atomic oxygen atoms. This is a direct extension of the physical picture proposed previously¹² and expounded on elsewhere in the context of hydroxyl-terminated CNPs.²⁶ Effectively, for small enough nanoparticles, a critical size is reached when O_x^q molecules, with variable oxidation states, better accommodate the coordination desired by surface cations on nonstoichiometric faces, edges, and corners.¹² Therefore, any metal oxide nanoparticle with exposed nonstoichiometric faces, edges, or corners should be expected to exhibit the size-dependent transformation in surface configuration invoked here. Therefore, the synthesis of sufficiently small, superoxidized nano-

particles is likely a general approach for the fabrication of metal oxide catalysts with enhanced surface densities of active sites.

■ ASSOCIATED CONTENT

● Supporting Information

The Supporting Information is available free of charge on the ACS Publications website at DOI: [10.1021/acs.chemmater.5b02426](https://doi.org/10.1021/acs.chemmater.5b02426).

Materials and methods of synthesizing oxidized 5 and 30 nm cubic ceria nanoparticles as well as 5 and 15 nm polyhedral ceria nanoparticles; characterization of fabricated ceria nanoparticles ([PDF](#))

■ AUTHOR INFORMATION

Corresponding Authors

*(X.H.) E-mail: xhu224@uky.edu.

*(M.J.B.) E-mail: m.beck@uky.edu.

Notes

The authors declare no competing financial interest.

■ ACKNOWLEDGMENTS

The authors thank Dr. T. John Balk, Dr. Eric A. Grulke, and Dr. J. Zach Hilt from Department of Chemical and Materials Engineering at the University of Kentucky for access to and use of their lab equipment.

■ REFERENCES

- Panhans, M. A.; Blumenthal, R. N. A Thermodynamic and Electrical Conductivity Study of Nonstoichiometric Cerium Dioxide. *Solid State Ionics* **1993**, *60*, 279–298.
- Carrettin, S.; Concepción, P.; Corma, A.; López Nieto, J. M.; Puntes, V. F. Nanocrystalline CeO_2 Increases the Activity of Au for CO Oxidation by Two Orders of Magnitude. *Angew. Chem., Int. Ed.* **2004**, *43*, 2538–2540.
- Rodriguez, J. A.; Graciani, J.; Evans, J.; Park, J. B.; Yang, F.; Stacchiola, D.; Senanayake, S. D.; Ma, S.; Pérez, M.; Liu, P.; Fdez Sanz, J.; Hrbek, J. Water-Gas Shift Reaction on a Highly Active Inverse $CeO_x/Cu(111)$ Catalyst: Unique Role of Ceria Nanoparticles. *Angew. Chem., Int. Ed.* **2009**, *48*, 8047–8050.
- Primo, A.; Marino, T.; Corma, A.; Molinari, R.; García, H. Efficient Visible-Light Photocatalytic Water Splitting by Minute Amounts of Gold Supported on Nanoparticulate CeO_2 Obtained by a Biopolymer Templating Method. *J. Am. Chem. Soc.* **2011**, *133*, 6930–6930.
- Gaudillère, C.; Vernoux, P.; Mirodatos, C.; Caboche, G.; Farrusseng, D. Screening of Ceria-Based Catalysts for Internal Methane Reforming in Low Temperature SOFC. *Catal. Today* **2010**, *157*, 263–269.
- Huang, M.; Fabris, S. CO Adsorption and Oxidation on Ceria Surfaces from DFT+U Calculations. *J. Phys. Chem. C* **2008**, *112*, 8643–8648.
- Huang, Y. Q.; Wang, A. Q.; Li, L.; Wang, X. D.; Su, D. S.; Zhang, T. Ir-in-ceri": A highly selective catalyst for preferential CO oxidation. *J. Catal.* **2008**, *255*, 144–152.
- Aneggi, E.; Wiater, D.; de Leitenburg, C.; Llorca, J.; Trovarelli, A. Shape-Dependent Activity of Ceria in Soot Combustion. *ACS Catal.* **2014**, *4*, 172–182.
- Migani, A.; Vayssilov, G. N.; Bromley, S. T.; Illas, F.; Neyman, K. M. Dramatic Reduction of the Oxygen Vacancy Formation Energy in Ceria Particles: A Possible Key to Their Remarkable Reactivity at the Nanoscale. *J. Mater. Chem.* **2010**, *20*, 10535–10546.
- Xu, J.; Harmer, J.; Li, G.; Chapman, T.; Collier, P.; Longworth, S.; Tsang, S. C. Size Dependent Oxygen Buffering Capacity of Ceria Nanocrystals. *Chem. Commun.* **2010**, *46*, 1887–1889.

- (11) Kullgren, J.; Hermansson, K.; Broqvist, P. Supercharged Low-Temperature Oxygen Storage Capacity of Ceria at the Nanoscale. *J. Phys. Chem. Lett.* **2013**, *4*, 604–608.
- (12) Huang, X.; Beck, M. J. Surface Structure of Catalytically-Active Ceria Nanoparticles. *Comput. Mater. Sci.* **2014**, *91*, 122–133.
- (13) Li, C.; Domen, K.; Maruya, K.; Onishii, T. Dioxygen Adsorption on Well-Outgassed and Partially Reduced Cerium Oxide Studied by FT-IR. *J. Am. Chem. Soc.* **1989**, *111*, 7683–7687.
- (14) Haneda, M.; Mizushima, T.; Kakuta, N. Behaviour of Oxygen Species Adsorbed on Al_2O_3 -Supported Cerium Oxide Catalysts for Methane Oxidation. *J. Chem. Soc., Faraday Trans.* **1995**, *91*, 4459–4465.
- (15) Binet, C.; Daturi, M.; Lavalley, J. C. IR Study of Polycrystalline Ceria Properties in Oxidised and Reduced States. *Catal. Today* **1999**, *50*, 207–225.
- (16) Soria, J.; Coronado, J.; Conesa, J. C. Spectroscopic Study of Oxygen Adsorption on $\text{CeO}_2/\gamma\text{-Al}_2\text{O}_3$ Catalyst Supports. *J. Chem. Soc., Faraday Trans.* **1996**, *92*, 1619–1626.
- (17) Soria, J.; Martinez-Arias, A.; Conesa, J. C. Spectroscopic Study of Oxygen Adsorption as A Method to Study Surface Defects on CeO_2 . *J. Chem. Soc., Faraday Trans.* **1995**, *91*, 1669–1678.
- (18) Bozon-Verduraz, F.; Bensalem, A. IR Studies of Cerium Dioxide: Influence of Impurities and Defects. *J. Chem. Soc., Faraday Trans.* **1994**, *90*, 653–657.
- (19) Pushkarev, V. V.; Kovalchuk, V. I.; d'Itri, J. L. Probing Defect Sites on the CeO_2 Surface with Dioxygen. *J. Phys. Chem. B* **2004**, *108*, 5341–5348.
- (20) Wu, Z. L.; Li, M. J.; Howe, J.; Meyer, H. M., III; Overbury, S. H. Probing Defect Sites on CeO_2 Nanocrystals with Well-Defined Surface Planes by Raman Spectroscopy and O_2 Adsorption. *Langmuir* **2010**, *26*, 16595–16606.
- (21) Bulanin, K. M.; Lavalley, J. C.; Tsyganenko, A. A. IR Spectra of Adsorbed Ozone. *Colloids Surf., A* **1995**, *101*, 153–158.
- (22) Bulanin, K. M.; Lavalley, J. C.; Lamotte, J.; Mariey, L.; Tsyganenko, M. N.; Tsyganenko, A. A. Infrared Study of Ozone Adsorption on CeO_2 . *J. Phys. Chem. B* **1998**, *102*, 6809–6816.
- (23) Preda, G.; Migani, A.; Neyman, K. M.; Bromley, S. T.; Illas, F.; Pacchioni, G. Formation of Superoxide Anions on Ceria Nanoparticles by Interaction of Molecular Oxygen with Ce^{3+} Sites. *J. Phys. Chem. C* **2011**, *115*, 5817–5822.
- (24) Inerbaev, T. M.; Seal, S.; Masunov, A. E. Density Functional Study of Oxygen Vacancy Formation and Spin Density Distribution in Octahedral Ceria Nanoparticles. *J. Mol. Model.* **2010**, *16*, 1617–1623.
- (25) Trovarelli, A. Catalytic Properties of Ceria and CeO_2 -Containing Materials. *Catal. Rev.: Sci. Eng.* **1996**, *38*, 439–520.
- (26) Huang, X.; Beck, M. J. Determining the Oxidation State of Small, Hydroxylated Metal-Oxide Nanoparticles with Infrared Absorption Spectroscopy. *Chem. Mater.* **2015**, *27*, 2965–2972.

■ NOTE ADDED AFTER ASAP PUBLICATION

This paper was published ASAP on August 26, 2015, with errors to the first page, Figure 2, Table 1, and the Acknowledgment Section. The corrected version was reposted with the issue on September 8, 2015.